Improvement of Phase Stability and Accurate Determination of Optical Constants of SnO Thin Films by Using Al_2O_3 Capping Layer

Ling Yan Liang, Zhi Min Liu, Hong Tao Cao,* Yuan Yuan Shi, Xi lian Sun, Zheng Yu, Ai Hua Chen, Hai Zhong Zhang, and Yan Qun Fang

Division of Functional Materials and Nano Devices, Ningbo Institute of Material Technology and Engineering, Chinese Academy of Sciences, Ningbo 315201, People's Republic of China

LETTER

ABSTRACT In this letter, it is proposed that the usage of Al_2O_3 capping layer can tremendously improve the phase stability of SnO thin films, which allows the accurate determination of the optical constants of the SnO films without the perturbation arising from impurity phases. For the SnO films, the refraction index and extinction coefficient are significantly influenced by the crystallinity. The nondirect optical bandgap of the amorphous SnO films is determined to be 2.27 eV, whereas two nondirect optical transitions are observed in the polycrystalline SnO films and the corresponding gap energies are estimated to be 0.50 and 2.45 eV, respectively.

KEYWORDS: tin monoxide • disproportionation • oxygen chemical potential • spectroscopic ellipsometry • polarizability

INTRODUCTION

Tin monoxide (SnO) has been studied as the anode material (1), gas sensitive material (2), coating substance (3), catalyst (3), precursor to produce tin oxide (SnO_2) (4), and semiconductor layers of p-channel thin film transistors (TFTs) (5). Up to now, the TFTs employing SnO channels exhibited the highest field effect mobility (~ 1 cm^2 V^{-1} s^{-1}) among the reported values for p-channel oxide TFTs (6). In spite of these wide applications, very few reports have been published so far on the refraction index n and extinction coefficient k of SnO thin films. Moreover, the band structure calculations have shown that SnO has a nondirect fundamental gap (7), but most experimenters regarded the SnO as a direct bandgap material to study its optical bandgap (5, 8). The accurate determination of these optical constants is based on a prerequisite of the availability of pure SnO films. However, some researchers found that SnO phase commenced the transformation into SnO_2 phase and/or intermediate oxide phase (Sn_2O_3 or Sn_3O_4) with the expulsion of Sn atoms (i.e., the disproportionation reaction) above 300 °C on heating (3, 4), and outmost oxidation always took place in O_2-contained ambient because the oxidation from SnO to SnO_2 is spontaneous based on the standard Gibbs energy of formation (9, 10).These phase instabilities of SnO put a burden on pure SnO film preparation and accurate determination of its physical properties, hence limiting its technological applications.

Our previous study has suggested that packaging or surface passivation is necessary to avoid the oxidization of SnO, and SnO samples with smaller specific surface areas exhibit a lower disproportionation rate on heating (10). On the basis of these considerations, a capping layer could be employed to protect SnO thin films from oxidizing and decomposing. Generally, Al_2O_3 is known as a chemically stable material with a small oxygen diffusion coefficient (5×10^{-25} cm^2/s at 950 °C) and a wide bandgap (8.8 eV) (11). In this work, Al_2O_3 capping layers were deposited to improve the phase stability of SnO films, then the optical properties of the SnO films were analyzed via spectroscopic ellipsometry (SE), which is a forcible method to acquire optical constants of oxide thin films and especially to study their nondirect optical transitions (12, 13).

* Corresponding author. E-mail: h_cao@nimte.ac.cn.
Received for review March 18, 2010 and accepted May 18, 2010
DOI: 10.1021/am100236s
2010 American Chemical Society

EXPERIMENTAL DETAILS

SnO thin films with or without Al_2O_3 capping layers were deposited on single-side-polished quartz in an e-beam evaporation system. After evacuating to 5.0×10^{-5} Pa, amorphous SnO thin films were evaporated from a high-purity SnO_2 source with a deposition rate of 2.4 nm/min at 250 °C. Thirty-nanometer-thick Al_2O_3 thin films as the capping layers were then deposited at room temperature on half of the as-deposited (as-dep.) SnO films by the same e-beam evaporation system. And then, some SnO thin films (with or without Al_2O_3 capping layers) were selected to undergo rapid thermal annealing (RTA) at temperatures ranging from 300 to 650 °C for 10 min in Ar ambient. In addition, some Al_2O_3-capped SnO samples were subjected to RTA treatment separately in air and O_2 ambient at 650 °C for 10 min.

The phase identification of the prepared films were carried out by using a multipurpose X-ray diffractometer (Bruker, D8 Advance) working with Cu−K_α radiation. The optical properties of the Al_2O_3-capped SnO films were measured via a variable angle spectroscopic ellipsometer (J.A.Woollam Co., Inc.) in the UV−vis−NIR range from 0.73 to 6.20 eV. The ellipsometric angle ψ and phase difference Δ were recorded at incidence angles of 55, 65, and 75°, respectively.

RESULTS AND DISCUSSION

Figure 1 presents X-ray diffraction (XRD) patterns in $\theta-2\theta$ scans of the bare SnO films annealed in Ar ambient.

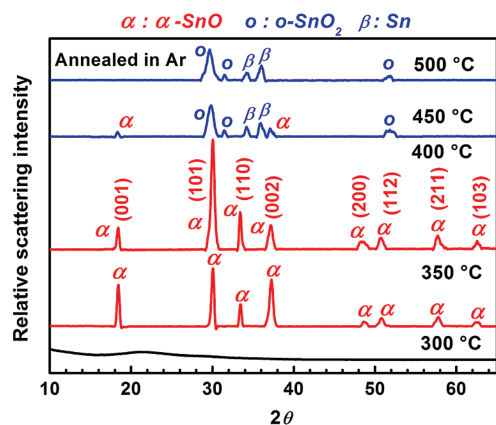

FIGURE 1. XRD patterns of the bare SnO films annealed from 300 to 500 °C in Ar ambient.

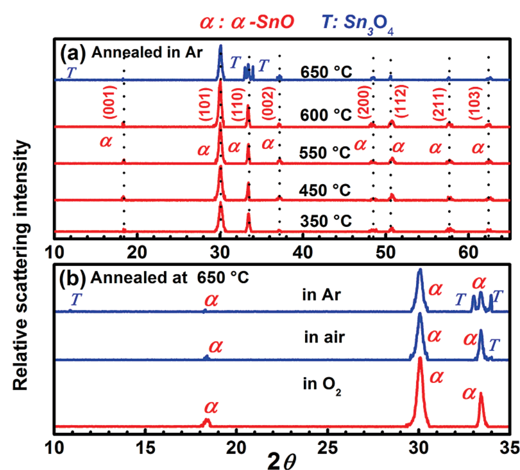

FIGURE 2. XRD patterns of the Al_2O_3-capped SnO films (a) annealed from 350 to 650 °C in Ar ambient; (b) annealed at 650 °C in Ar, air, and O_2 ambient, respectively. For clarity, only the patterns in a 2θ range of 10−35° are shown in b.

For the 300 °C annealed SnO film, only the halo from the quartz substrate is observed, indicating the amorphous nature of the film. For the 350 and 400 °C annealed SnO films, there are eight sharp diffraction peaks, which correspond to the reflections of α-SnO phase (labeled with α, tetragonal litharge structure, JCPDS card no. 06−0395). Upon annealing at temperatures above 400 °C, the SnO peaks become weaker and disappear totally at 500 °C, whereas some new peaks that can be indexed to orthorhombic SnO_2 (labeled with o, JCPDS card no. 29−1484) and metallic Sn (labeled with β, JCPDS card no. 19−1365) are present and become dominated, suggesting that the bare SnO film becomes unstable when heated at temperatures above 400 °C. Similarly, the 300 °C annealed SnO film with the capping layer is also amorphous. Nevertheless, for the 350−600 °C annealed SnO films with the capping layer, only the SnO phase can be identified and the intensity of the α-SnO (101) peak located at 29.9° increases with increasing annealing temperature, as shown in Figure 2a. When annealed at 650 °C in Ar ambient, the SnO (101) peak gets attenuated and three new reflections which can be indexed to Sn_3O_4 (labeled with T, JCPDS card no. 20−1293) phase are observed (see Figure 2a), implying the occurrence of the disproportionation of SnO. In particular for the case of 650 °C annealing in O_2-contained ambient (see Figure 2b), however, the Sn_3O_4 peaks become very weak in air ambient and eventually disappear in O_2 ambient, with the SnO peaks remaining solely.

With the goal of improving the phase stability of SnO, the utilization of the capping layer together with the O_2-contained annealing ambient is proposed, which has been validated from the aforementioned experimental results. It is speculated that the oxygen chemical potential near the bare SnO film drops sharply under heating in Ar ambient, giving rise to a large oxygen vacancy concentration (14), which may induce an internal displacement of oxygen in SnO lattice (disproportionation reaction) and eventually deteriorate the phase stability. As a result, how to tune the oxygen chemical potential near the SnO surface is an essential prerequisite to address the issue of phase stability. On one hand, the Al_2O_3 capping layer is believed to mitigate the severe variation of the surface oxygen chemical potential and promote the phase stability of the SnO films (as seen in Figure 1 and Figure 2a). On the other hand, the oxygen chemical potential varies under different chemical atmosphere (e.g., Ar, air, and pure O_2), i.e., it increases with increasing oxygen partial pressure (14). It is noteworthy, however, that increasing the oxygen partial pressure alone cannot help to solve the problem, because the oxidation from SnO to SnO_2 is spontaneous according to the thermodynamics theory (9). Therefore, the usage of the O_2-contained annealing ambient must work together with the capping layer to obtain SnO single phase.

The improvement of phase stability of SnO films allows us to obtain their optical constants, effectively circumventing the perturbation from impurity phases. In this work, the optical properties of the Al_2O_3-capped SnO samples were studied by SE. A simple four-phase model consisting of quartz substrate/SnO thin film/Al_2O_3 thin film/surface rough layer (50% Al_2O_3 + 50% void) has been used to represent the sample, as shown in the insert of Figure 3. The Tauc−Lorentz (TL) dispersion function is employed to characterize the dielectric function of the SnO films, which is expressed as follows (12)

$$\varepsilon_2(E) = \begin{cases} \dfrac{AE_0C(E - E_g)^2}{(E^2 - E_0^2)^2 + C^2E^2}\dfrac{1}{E}, & (E > E_g) \\ 0, & (E \le E_g) \end{cases} \tag{1}$$

and

$$\varepsilon_1(E) = \varepsilon_\infty + \frac{2}{\pi}P\int_{E_g}^{\infty}\frac{\xi\varepsilon_2(\xi)}{\xi^2 - E^2}d\xi \tag{2}$$

where the parameters A, E_0, C, E_g, ε_∞, and P are the amplitude, peak transition energy, broadening term, band gap, high frequency dielectric constant, and Cauchy principal part of the integral, respectively. Cauchy dispersion relation and the empirical Urbach relation were used to generate the optical constants of Al_2O_3 (15). The quality of the fit was

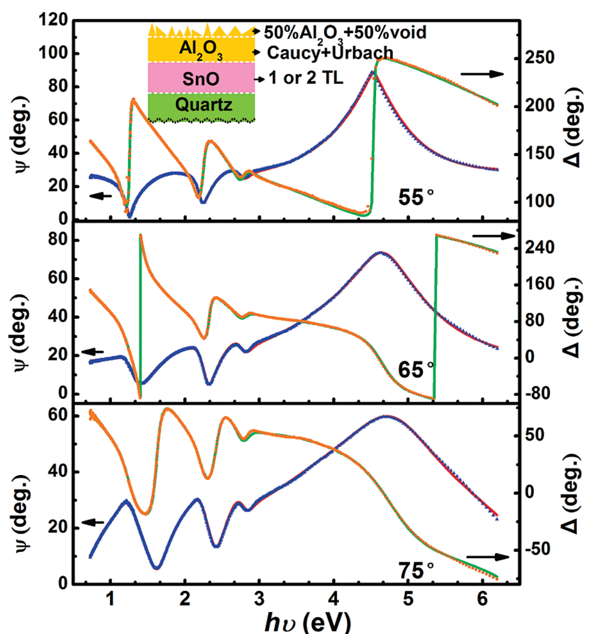

FIGURE 3. Experimental (symbols) and fitted (solid curves) ψ and Δ of the Al_2O_3-capped SnO film annealed at 450 °C. The inset presents the optical model used to fit the ellipsometry data.

Table 1. TL Parameter Values for Fitting the Optical Functions of the Al_2O_3-Capped SnO Films[a]

sample	t_{SnO}	E_{g1}	A_1	E_{01}	C_1	E_{g2}	A_2	E_{02}	C_2	MSE	n
as-dep.	235.5					2.18	100.3	3.86	3.46	5.920	2.54
300/Ar	228.9					2.23	107.3	3.85	3.38	5.201	2.54
350/Ar	209.9	0.0001	3.623	3.55	0.86	2.63	376.9	2.63	2.35	5.816	2.76
450/Ar	203.2	0.0001	3.646	3.54	0.79	2.63	397.2	2.62	2.28	5.962	2.81
550/Ar	198.3	0.0001	4.980	3.56	0.78	2.62	374.1	2.68	2.24	5.108	2.82
600/Ar	197.1	0.0001	4.690	3.59	0.81	2.62	384.4	2.60	2.64	5.588	2.84
$650/O_2$	198.5	0.0001	5.088	3.62	0.85	2.62	419.8	2.61	2.98	5.500	2.84

[a] The subscripts 1 and 2 stand for the first and second TL function, respectively. t_{SnO} and MSE are the SnO film thickness and mean-square error, respectively. The n values at $\lambda = 550$ nm are also listed.

assessed by the evaluation of the mean-squared error (MSE) function (16). It is found that the fitting quality is acceptable when one TL dispersion function is used for the as-dep. and 300 °C annealed films, whereas two TL dispersion functions are needed for the films annealed at higher temperatures, indicating that more than one single type of electronic transition dominate the optical absorption for the polycrystalline SnO films (12).

Figure 3 shows the representative experimental (symbols) and fitted (solid curves) spectroscopic spectra of ψ and Δ as a function of photon energy ($h\nu$) for the Al_2O_3-capped SnO film annealed at 450 °C. The spectra of the other samples with smaller fitting MSE values are not exhibited here. It can be seen that a good agreement between the experimental and fitting spectra is obtained over the studied range, revealing that the TL dispersion function and the four-phase model work well and the optical properties of the SnO can be exactly determined by the best fitting results. Table 1 summarizes the SnO layer thicknesses and the TL parameter values obtained from data fitting with a 90% confidence limit.

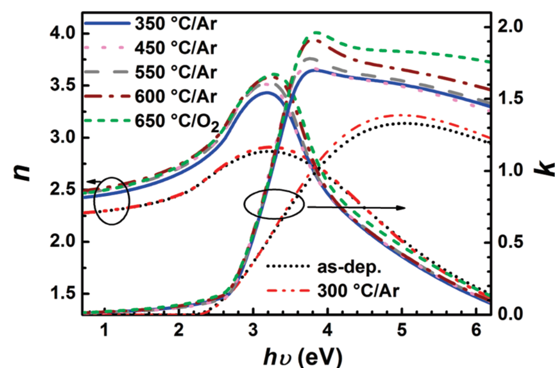

FIGURE 4. Refractive index (n) and extinction coefficient (k) of the Al_2O_3-capped SnO films. The data of the sample annealed at 650 °C in O_2 ambient are chosen because of the pure SnO phase according to XRD results.

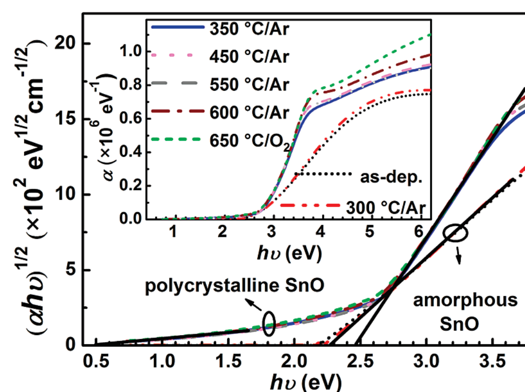

FIGURE 5. Plots of $(\alpha h\nu)^{1/2}$ vs $h\nu$ for the Al_2O_3-capped SnO films. The inset plots the absorption coefficient α vs $h\nu$.

The extracted optical constants n and k for the Al_2O_3-capped SnO films are presented in Figure 4. The n value is 2.54 at $h\nu = 2.25$ eV (i.e., the wavelength $\lambda = 550$ nm) for the as-dep. and 300 °C annealed SnO films (amorphous SnO films), and then increases by 0.2−0.3 for the films annealed at higher temperatures (polycrystalline SnO films), as listed in Table 1. It is found that the optical constants of SnO films are significantly influenced by their crystallinity. Compared to the amorphous SnO films, the polycrystalline films have larger n values in the photon energy region 0.73−3.84 eV but smaller n above 3.84 eV. The opposite variation trends of n between low and high photon energy regions are related to the local polarizability, and specifically the bigger n in lower photon energy region is always associated with the larger polarizability (17, 18). It implies that the crystallization process by thermal annealing establishes the long-range ordering of atoms and then enhances the local polarizability of SnO to a certain degree, which is also the case for other IV−VI compounds, such as PbS, SnTe, etc. (18, 19).

The extinction coefficient of the Al_2O_3-capped SnO films increases as the annealing temperature increases (see Figure 4). The absorption coefficients α can be obtained via $\alpha = 4\pi k/\lambda$, as depicted in the inset of Figure 5. It is observed that α of the polycrystalline SnO films rises more rapidly than that of the amorphous ones, achieving the values from 7×10^5 to 10^6 cm^{-1} (amorphous to polycrystalline) in the UV region. Based on the optical absorption spectra, the nature of optical transition can be determined. Since SnO systems

LETTER

have a nondirect fundamental gap (7), the interband absorption can be expressed by the equation $\alpha h\nu \propto (h\nu - E_g)^2$. The variation of $(\alpha h\nu)^{1/2}$ with $h\nu$ for the Al_2O_3-capped SnO films is shown in Figure 5. The E_g values are determined from the energy intercept by extrapolating the linear portion of the plot of $(\alpha h\nu)^{1/2}$ versus $h\nu$ to $\alpha = 0$. For the amorphous SnO films, the nondirect bandgap is estimated to be 2.27 eV, whereas for the polycrystalline ones, two electronic transitions dominate the optical absorption and the corresponding gap energies are obtained to be 0.50 and 2.45 eV, respectively, of which the small gap energy (0.50 eV) is in between the reported nondirect optical bandgap (0.7 eV) of SnO powder samples and the theoretical value (0.3 eV) (7, 20). It is revealed that the gap values for SnO are strongly correlated to its amorphous or crystalline state, almost regardless of the annealing temperatures (Figure 5). Thus, the emergence of the two optical transitions in the polycrystalline SnO films might result from the change in film structures, which induces the increase of singularities in the interband density of states of the films. In general, these increased singularities are caused by the presence of long-range ordering in polycrystalline or crystalline films that are absent in their amorphous counterpart. Similar characteristics were reported elsewhere for Ta_2O_5 films and HfO_2 films (13, 21).

CONCLUSIONS

In conclusion, the phase stability and optical properties of SnO films with Al_2O_3 capping layers have been investigated. The phase stability of the SnO films can be tremendously improved via the usage of the capping layer together with O_2-contained ambient, which can modify the surface oxygen chemical potential of the SnO films. Good fit of the ellipsometry data is realized by employing either one or two TL dispersion functions. It is suggested that the establishment of long-range ordering during crystallization enhances the local polarizability of the SnO films, hence increasing the refractive index in the range of 0.73−3.84 eV. The nondirect optical bandgap of the amorphous SnO films is estimated to be 2.27 eV, whereas for the polycrystalline ones, two nondirect optical energy gaps are determined to be 0.50 and 2.45 eV, respectively. The unusual optical characteristic of the polycrystalline films is believed to stem from the increase in singularities in the interband intensity of states by crystallization.

Acknowledgment. This work is partially supported by the key project of the Natural Science Foundation of Zhejiang province, P. R. China (Grant 0804201051), an Innovative Research International Partnership Project of Chinese Academy of Sciences, and the Special Foundation of President of Chinese Academy of Sciences (Grant 080421WA01).

REFERENCES AND NOTES

(1) Ning, J. J.; Jiang, T.; Men, K. K.; Dai, Q. Q.; Li, D. M.; Wei, Y. J.; Liu, B. B.; Chen, G.; Zou, B.; Zou, G. T. *J. Phys. Chem. C* **2009**, *113*, 14140–14144.
(2) Calderer, J.; Molinas, P.; Sueiras, J.; Llobet, E.; Vilanova, X.; Correig, X.; Masana, F.; Rodriguez, A. *Microelectron. Reliab.* **2000**, *40*, 807–810.
(3) Giefers, H.; Porsch, F.; Wortmann, G. *Solid State Ionics* **2005**, *176*, 199–207.
(4) Pan, X. Q.; Fu, L. *J. Appl. Phys.* **2001**, *89*, 6048–6055.
(5) Guo, W.; Fu, L.; Zhang, Y.; Zhang, K.; Graham, G.; Liang, L. Y.; Liu, Z. M.; Cao, H. T.; Pan, X. Q. *Appl. Phys. Lett.* **2010**, *96*, 042113 (3pp).
(6) Matsuzaki, K.; Nomura, K.; Yanagi, H.; Kamiya, T.; Hirano, M.; Hosono, H. *Phys. Status Solidi A* **2009**, *206*, 2192–2197.
(7) Togo, A.; Oba, F.; Tanaka, I.; Tatsumi, K. *Phys. Rev. B* **2006**, *74*, 195128 (8pp).
(8) Geurts, J.; Rau, S.; Richter, W.; Schmitte, F. J. *Thin Solid Films* **1984**, *121*, 217–225.
(9) Liang, L. Y.; Liu, Z. M.; Cao, H. T.; Pan, X. Q. *ACS Appl. Mater. Interfaces* **2010**, *2*, 1060–1065.
(10) Moreno, M. S.; Punte, G.; Rigotti, G.; Mercader, R. C.; Weisz, A. D.; Blesa, M. A. *Solid State Ionics* **2001**, *144*, 81–86.
(11) Green, M. L.; Gusev, E. P.; Degraeve, R.; Garfunkel, E. L. *J. Appl. Phys.* **2001**, *90*, 2057–2121.
(12) Lu, H. L.; Scarel, G.; Alia, M.; Fanciulli, M.; Ding, S. J.; Zhang, D. W. *Appl. Phys. Lett.* **2008**, *92*, 222907 (3pp).
(13) Cho, Y. J.; Nguyen, N. V.; Richter, C. A.; Ehrstein, J. R.; Lee, B. H.; Lee, J. C. *Appl. Phys. Lett.* **2002**, *80*, 1249–1251.
(14) Forst, C. J.; Ashman, C. R.; Schwarz, K.; Blochl, P. E. *Nature* **2004**, *427*, 53–56.
(15) Yang, S. H.; Liu, Y.; Zhang, Y. L.; Mo, D. *Surf. Interface Anal.* **2009**, *41*, 502–507.
(16) Paulson, P. D.; Hegedus, S. S. *J. Appl. Phys.* **2004**, *96*, 5469–5477.
(17) Pan, S. S.; Zhang, Y. X.; Teng, X. M.; Li, G. H.; Li, L. *J. Appl. Phys.* **2008**, *103*, 093103 (4pp).
(18) Shportko, K.; Kremers, S.; Woda, M.; Lencer, D.; Robertson, J.; Wuttig, M. *Nat. Mater.* **2008**, *7*, 653–658.
(19) Littlewood, P. B. *J. Phys. C: Solid State Phys.* **1979**, *12*, 4459–4468.
(20) Ogo, Y.; Hiramatsu, H.; Nomura, K.; Yanagi, H.; Kamiya, T.; Hirano, M.; Hosono, H. *Appl. Phys. Lett.* **2008**, *93*, 032113 (3pp).
(21) Nguyen, N. V.; Richter, C. A.; Cho, Y. J.; Alers, G. B.; Stirling, L. A. *Appl. Phys. Lett.* **2000**, *77*, 3012–3014.

AM100236S